nature cell biology

Ciliary entry of the kinesin-2 motor KIF17 is regulated by importin-β2 and RanGTP

John F. Dishinger[1], Hooi Lynn Kee[1], Paul M. Jenkins[2], Shuling Fan[3], Toby W. Hurd[5], Jennetta W. Hammond[1], Yen Nhu-Thi Truong[2], Ben Margolis[3,4], Jeffrey R. Martens[2] and Kristen J. Verhey[1]

The biogenesis, maintenance and function of primary cilia are controlled through intraflagellar transport (IFT) driven by two kinesin-2 family members, the heterotrimeric KIF3A/KIF3B/KAP complex and the homodimeric KIF17 motor[1,2]. How these motors and their cargoes gain access to the ciliary compartment is poorly understood. Here, we identify a ciliary localization signal (CLS) in the KIF17 tail domain that is necessary and sufficient for ciliary targeting. Similarities between the CLS and classic nuclear localization signals (NLSs) suggest that similar mechanisms regulate nuclear and ciliary import. We hypothesize that ciliary targeting of KIF17 is regulated by a ciliary-cytoplasmic gradient of the small GTPase Ran, with high levels of GTP-bound Ran (RanGTP) in the cilium. Consistent with this, cytoplasmic expression of GTP-locked Ran(G19V) disrupts the gradient and abolishes ciliary entry of KIF17. Furthermore, KIF17 interacts with the nuclear import protein importin-β2 in a manner dependent on the CLS and inhibited by RanGTP. We propose that Ran has a global role in regulating cellular compartmentalization by controlling the shuttling of cytoplasmic proteins into nuclear and ciliary compartments.

The development of the primary cilium, a microtubule-based organelle projecting from the surface of nearly all cells, has been proposed to be a consequence of evolved motor-protein-based trafficking unique to eukaryotic cells[3]. Primary cilia have important roles in sensory functions, such as photoreception, renal functioning and odorant sensing, at single-cell and multi-cellular levels[4–6]. Defective biogenesis or functioning of cilia causes a variety of human diseases, collectively termed ciliopathies[7,8], with pathological conditions including cystic kidney disease, brain malformations and obesity.

Although they can respond to a variety of sensory stimulants, the basic structure of primary cilia is highly conserved. The core axoneme consists of a ring of nine doublet microtubules that extend from the mother centriole at the basal body[1,9]. Ciliary construction and maintenance proceeds through IFT of ciliary components along the axoneme by kinesin and dynein motors[9]. In *Caenorhabditis elegans*, IFT requires the coordinated efforts of heterotrimeric kinesin-2 (the KIF3A/KIF3B/KAP complex) and homodimeric OSM-3 motors[10,11]. KIF17, the vertebrate homologue of OSM-3, has been shown to function as a ciliary motor in zebrafish photoreceptors and mammalian olfactory sensory neurons[12–14].

How kinesin motors and their cargoes gain entry to the cilium is unknown. Ciliary entry is a selective process, as analysis across several species has identified a unique ciliary proteome[15]. Ciliary entry presumably requires the transport of proteins located near the basal body across the ciliary transition zone[16], which may function as a diffusion barrier separating the cytoplasm from the intraciliary compartment. IFT cargo proteins have been observed around the basal body[17] and transition fibres[18] in the initial segment of cilia.

To study ciliary targeting of KIF17 in mammalian cells, we expressed mCitrine (mCit)-tagged KIF17 in cell lines that generate primary cilia. KIF17 accumulated at the distal tip of the primary cilium in all cell lines tested, including neuronal (Odora rat olfactory sensory neurons[19]), epithelial (MDCK II canine kidney and hTERT-RPE human retinal pigment epithelia) and fibroblast (NIH3T3) cells (Fig. 1a). Localization to the distal cilium was confirmed by co-staining for acetylated and γ-tubulin to mark the cilium and basal body, respectively (Fig. 1b). Ciliary localization of tagged KIF17 was observed regardless of the epitope (mCit, Flag or Myc) or its position (amino- or carboxy-terminal) (data not shown).

To identify sequences in KIF17 required for ciliary localization, we created truncated forms of the motor (Fig. 1c–e and Supplementary Fig. 1a). Deletion of the C-terminal tail domain abolished ciliary localization (KIF17(1–846), Fig. 1c), suggesting that the tail domain contains sequences required for ciliary targeting. Further C-terminal truncations also failed to localize to cilia (Supplementary Fig. 1). Surprisingly, constructs containing the KIF17 stalk and tail domains (mCherry–KIF17(490–1029), Fig. 1d) or the KIF17 tail domain alone (Myc–KIF17(801–1028), Fig. 1e) localized predominantly to the nucleus (Fig. 1d, e). This suggests that similar mechanisms may control nuclear and ciliary targeting. Parallels

[1]Department of Cell and Developmental Biology, University of Michigan Medical School, Ann Arbor, Michigan 48109, USA. [2]Department of Pharmacology, University of Michigan Medical School, Ann Arbor, Michigan 48109, USA. [3]Department of Internal Medicine, University of Michigan Medical School, Ann Arbor, Michigan 48109, USA. [4]Department of Biological Chemistry, University of Michigan Medical School, Ann Arbor, Michigan 48109, USA. [5]Department of Paediatrics and Communicable Disease, Division of Paediatric Nephrology, University of Michigan Medical School, Ann Arbor, Michigan 48109, USA.
Correspondence should be addressed to K.J.V. (email: kjverhey@umich.edu)

Received 16 March 2010; accepted 14 May 2010; published online 6 June 2010; DOI: 10.1038/ncb2073

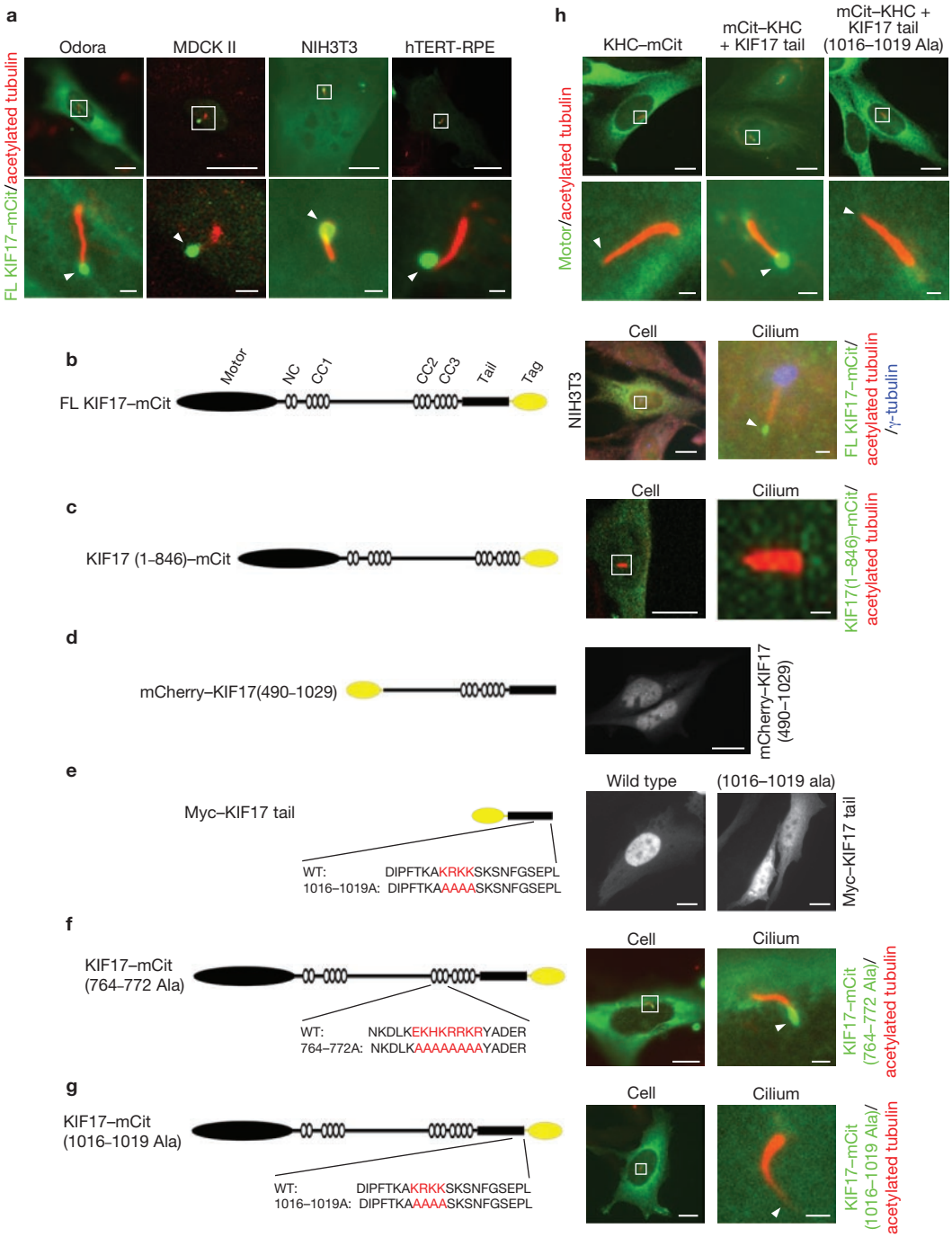

Figure 1 The KIF17 CLS is necessary and sufficient for ciliary localization. (**a**) Odora, MDCK II, NIH3T3 and hTERT-RPE cells expressing full-length (FL) KIF17–mCit (green) were fixed and stained for acetylated tubulin to mark cilia (red). Top row, images of entire cells; bottom row, higher magnifications of cilia in boxed areas. White arrowheads indicate distal tips of cilia. (**b**) Left, schematic of full-length human KIF17. NC, neck coil; CC, coiled coil. Right, NIH3T3 cells expressing KIF17–mCit (green) were fixed and stained for acetylated tubulin (red) to mark cilia and γ-tubulin (blue) to mark the basal body. (**c–g**) Schematics of truncated and mutant KIF17 constructs (left) and their localization in Odora cells (right). Cells expressing the indicated truncated or mutant KIF17 motors (green) were fixed and stained for acetylated tubulin (red in **c**,**f**,**g**) or the Myc tag (white in **d**). (**h**) Odora cells expressing full-length KHC–mCit or KHC fused with the wild-type or mutant versions of the KIF17 tail were fixed and stained with antibodies to acetylated tubulin (red). Scale bars are either 10 μm for images of an entire cell or 1 μm for images of cilia.

between nuclear and ciliary import have been suggested in the literature[20–22], but there is not yet any direct evidence.

To explore the possibility that ciliary entry of KIF17 uses mechanisms similar to nuclear import, we searched KIF17 for sequences resembling an NLS (ref. 23) and identified two potential sites: amino acids 767–772 (KRRKR) and 1016–1019 (KRKK). To test whether these sequences are necessary for KIF17 ciliary localization, we mutated the relevant residues to alanines in the full-length motor (Fig. 1f, g). Mutation of residues 764–772 in the KIF17 stalk did not affect ciliary localization (Fig. 1f), whereas mutation of residues 1016–1019 in the KIF17 tail

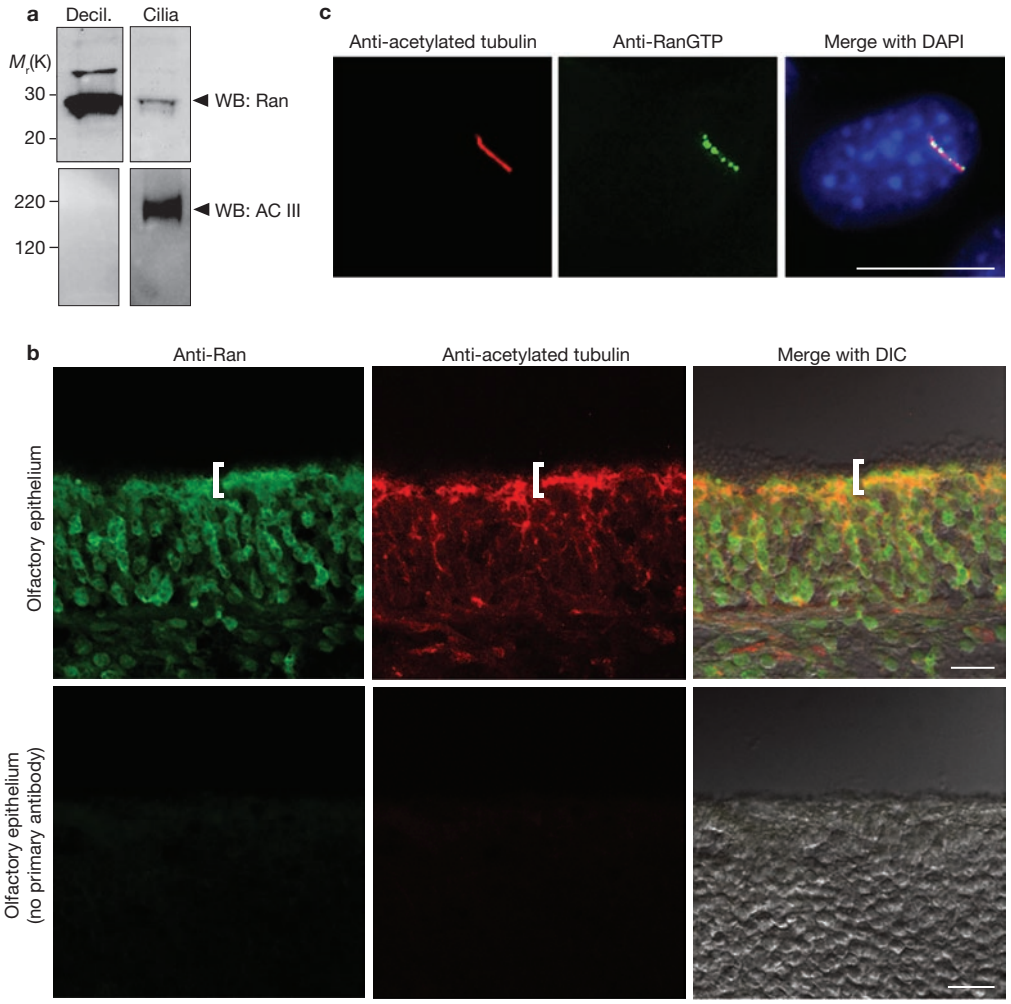

Figure 2 Ran is present in the ciliary compartment. (**a**) Primary cilia were isolated from rat olfactory epithelium and the presence of Ran and adenylyl cyclase III (AC III) in the ciliary (Cilia) and remaining deciliated (Decil.) fractions were determined by western blotting. Approximate molecular weights in kDa are shown on the left. Arrowheads designate protein of interest. Uncropped images of western blots are shown in Supplementary Fig. 7. (**b**) Representative compressed confocal stacks of coronal sections of rat nasal epithelia. Olfactory epithelia were immunostained with antibodies directed against Ran (left, green) and acetylated tubulin (middle, red). Merged image with differential interference contrast (DIC) image is shown on the right. Scale bar, 20 μm; brackets denote the cilia layer. Control images without primary antibody are shown below. (**c**) Immunofluorescence image of an NIH3T3 cell stained with anti-acetylated tubulin antibody (red), anti-RanGTP antibody (green) and 4,6-diamidino-2-phenylindole (DAPI; blue). Scale bar, 10 μm.

domain abolished ciliary localization (Fig. 1g). Identical results were obtained in other cell lines (Supplementary Fig. 2). These results indicate that the KRKK sequence in the KIF17 tail domain acts as a CLS. The KIF17 CLS can also function as an NLS, as mutation of residues 1016–1019 in the isolated KIF17 tail domain reduced the nuclear localization of this construct (Fig. 1e).

The observation that the CLS is necessary for ciliary localization of KIF17 (Fig. 1g) but is not sufficient for ciliary targeting when present in the isolated tail domain (Fig. 1e) indicates that there are likely to be several sequences in KIF17 that contribute to ciliary localization. To test whether the KIF17 CLS is sufficient for ciliary targeting of kinesin motors, we fused the tail domain (amino acids 801–1028) onto the C-terminus of a non-ciliary kinesin, the Kinesin-1 subunit kinesin heavy chain (KHC) (Fig. 1h). Fusion of the wild-type KIF17 tail domain resulted in ciliary localization of KHC, whereas fusion of the mutant KIF17 tail did not (Fig. 1h). This demonstrates that the KIF17 tail domain contains a CLS that is necessary and sufficient for ciliary targeting of kinesin motors.

Nuclear import involves recognition of NLSs by importin proteins, translocation through the nuclear pore complex (NPC) and dissociation of the NLS–importin complex in the nucleus by active GTP-bound forms of the small GTPase Ran (ref. 24). To investigate whether similar mechanisms regulate ciliary import of CLS-containing KIF17, we tested whether RanGTP is present in primary cilia and regulates trafficking of KIF17. Ran and importin proteins are present in ciliary proteomes from several species[15,25]. We found that Ran is present in a ciliary fraction isolated from rat olfactory tissue (Fig. 2a). Isolation of a ciliary-enriched fraction was confirmed by the presence of the ciliary protein adenylyl cyclase III (Fig. 2a) and scanning electron microscopy of olfactory tissue before and after removal of cilia (Supplementary Fig. 3a). Immunohistochemistry of rat olfactory (Fig. 2b) and respiratory (Supplementary Fig. 3b) epithelia also demonstrates that Ran is present in the cilia layer at the apical surface. The ciliary-localized Ran represents the active GTP-bound state of the protein, as both the cilium (Fig. 2c) and nucleus (Supplementary

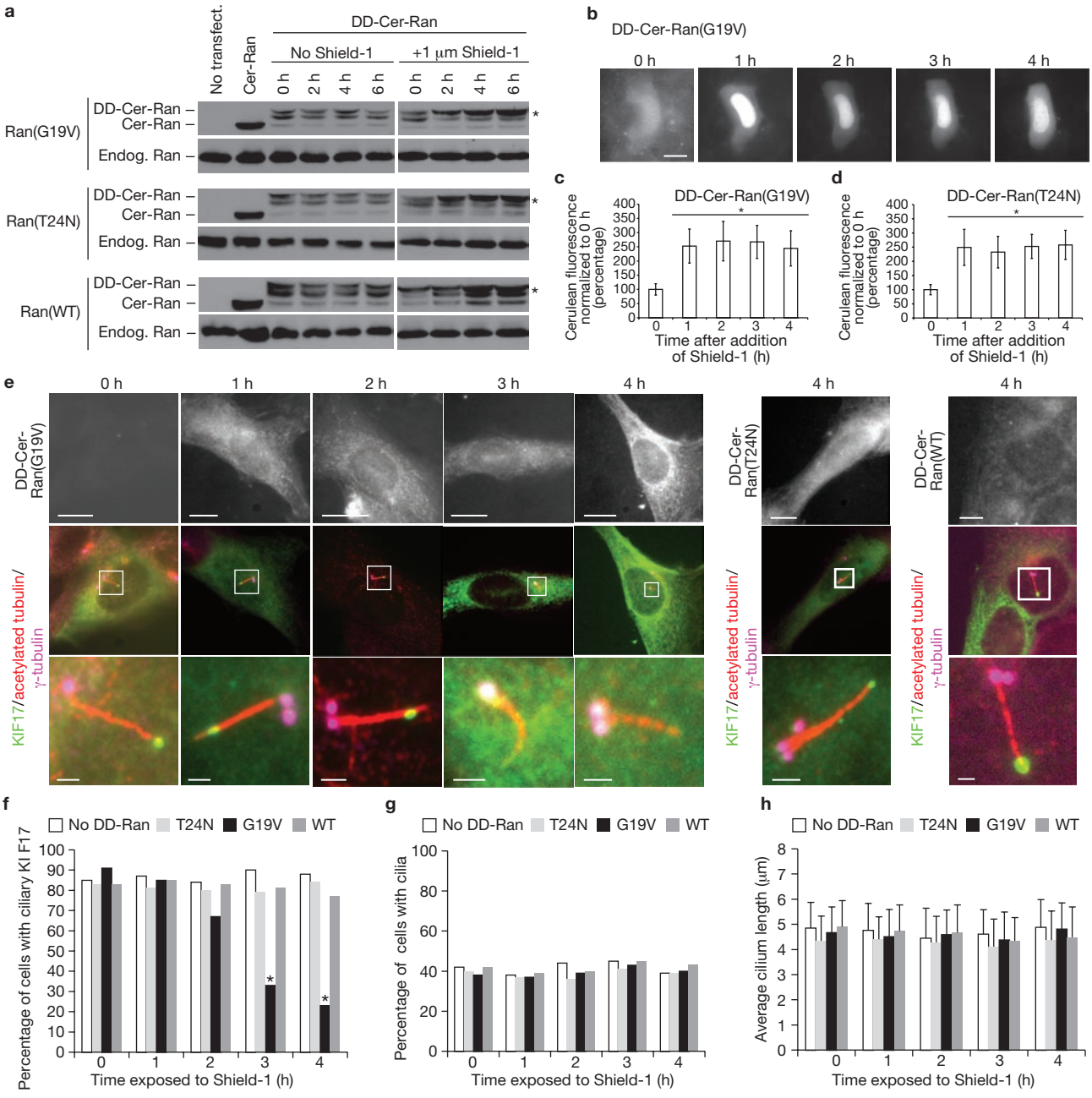

Figure 3 Fast upregulation of cytosolic RanGTP levels abolishes ciliary localization of KIF17. (**a**) COS cells expressing Cer-Ran (G19V, T24N or WT) or DD-Cer-Ran (G19V, T24N or WT) or untransfected control cells were exposed to Shield-1 for 0–6 h (right panels) or untreated (left panels). The expression of endogenous (endog.) and expressed Ran was determined by immunoblotting with an anti-Ran antibody. Uncropped images of western blots are shown in Supplementary Fig. 7. (**b–d**) Single cell analysis of live NIH3T3 cells expressing DD-Cer-Ran constructs following exposure to Shield-1. (**b**) Representative images of a single cell expressing DD-Cer-Ran(G19V) at 0–4 h of Shield-1 exposure. Scale bar, 10 μm. The fluorescence increase in multiple cells was quantified for (**c**) DD-Cer-Ran(G19V)-expressing cells ($n = 8$) and (**d**) DD-Cer-Ran(T24N)-expressing cells ($n = 10$). Quantification includes both nuclear and cytoplasmic fluorescence. $^*p < 0.05$ as compared to the 0 h time point (two-tailed Student's *t*-test). Data are presented as mean ± s.e.m. (**e**) NIH3T3 cells coexpressing DD-Cer-Ran(G19V) (left), DD-Cer-Ran(T24N) (middle) or KIF17–mCit and DD-Cer-Ran(WT) (right) were exposed to Shield-1 for 0–4 h and then fixed and stained for acetylated tubulin and γ-tubulin. (**f–h**) Quantification of the results in (**e**) to determine (**f**) the percentage of transfected cells with ciliary localization of KIF17–mCit ($n = 30$ for each time point, collected over three experiments), (**g**) the percentage of transfected cells with cilia ($n = 50$ for each) and (**h**) the cilium length in transfected cells ($n = 30$ for each). $^*p < 0.05$ as compared to 0 h of Shield-1 (Fisher's Exact test). Data are presented as mean ± s.d.

Fig. 4a) can be stained with an antibody that recognizes RanGTP but not RanGDP (ref. 26). These results are consistent with our proposal that a RanGTP/GDP gradient across the ciliary/cytoplasmic barrier regulates ciliary import.

To test whether ciliary RanGTP regulates KIF17 import, we coexpressed KIF17–mCit with Myc-tagged Ran proteins (wild-type (WT), a constitutively active GTP-bound G19V mutant and a T24N mutant that cannot bind nucleotide)[27]. We used serum-starved NIH3T3 cells to coexpress

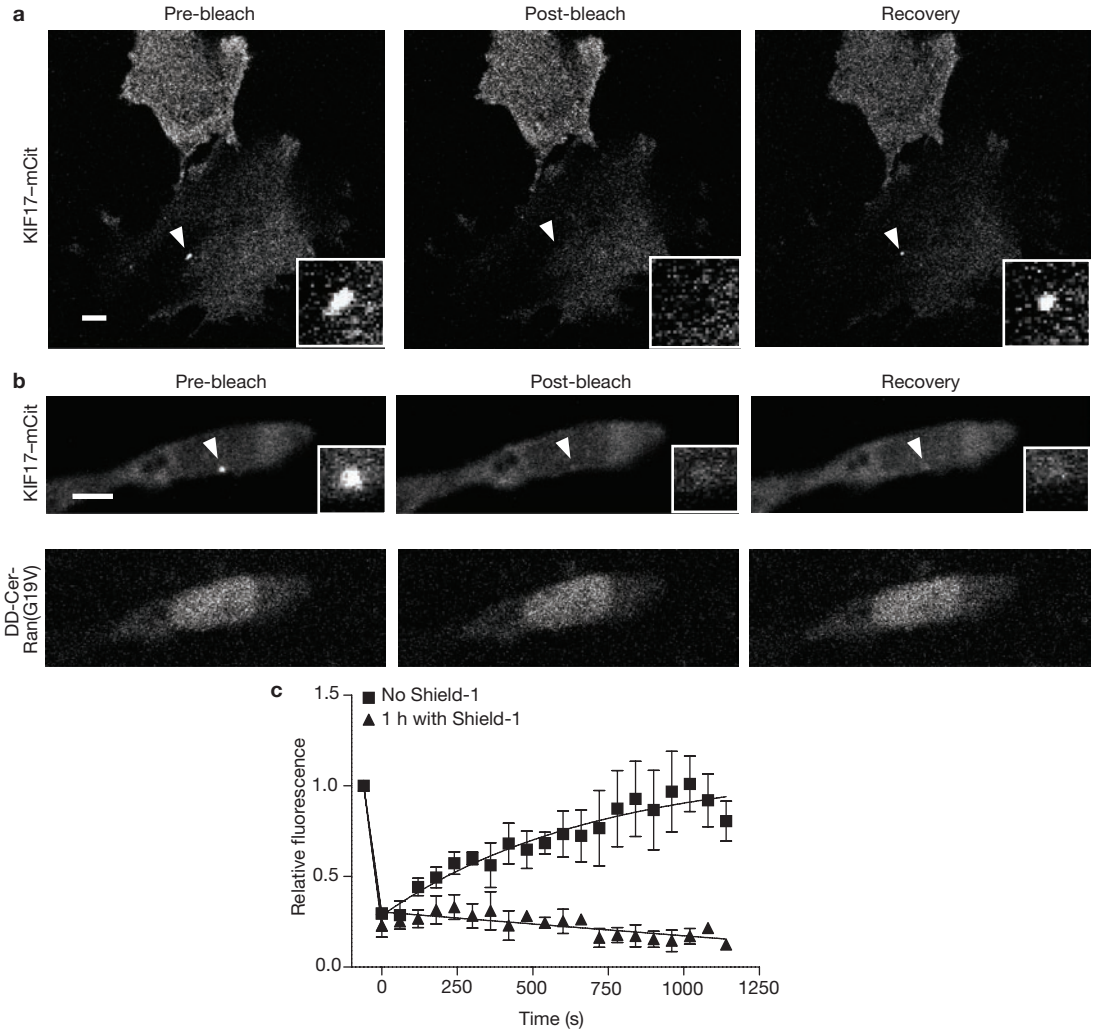

Figure 4 Upregulation of cytosolic RanGTP levels prevents ciliary entry of KIF17. FRAP analysis of Odora cells coexpressing KIF17–mCit and DD-Cer-Ran(G19V) in the (**a**) absence or (**b**) presence of Shield-1. The cells were imaged (pre-bleach) and the fluorescence in the distal tip of the cilium was then bleached at high laser power. The cells were again imaged (post-bleach) and the fluorescence recovery of KIF17–mCit in the cilium was monitored over time. White arrowheads, distal tips of cilia. Inset of each image is a close up of the cilium tip. Scale bars, 10 μm. (c) The fluorescence recovery of KIF17–mCit in the distal tips of cilia in the absence and presence of Shield-1 was quantified. Data are presented as mean ± s.e.m.; $n = 5$ for both traces. Data were fitted to a single exponential curve.

the exogenous proteins after cilia formation and limit any effects of Ran overexpression on ciliogenesis. Cytoplasmic expression of WT Ran or Ran(T24N) did not affect ciliary localization of KIF17, whereas expression of GTP-bound Ran(G19V) significantly reduced the number of cells with ciliary KIF17 without affecting cilia length (Supplementary Fig. 5).

To alleviate concerns that cytoplasmic expression of Ran proteins could indirectly affect ciliary targeting of KIF17, we developed a method for fast upregulation of Ran protein expression. The various Ran constructs were tagged with a destabilization domain (DD), which targets expressed proteins for rapid degradation. Addition of the cell-permeable ligand Shield-1 prevents protein degradation and allows rapid and continuous upregulation of protein levels[28–30]. Our DD-Ran constructs were also tagged with the fluorescent protein Cerulean (Cer). To verify the rapid expression of Ran proteins, lysates of COS cells expressing the DD-Cer-Ran plasmids and exposed to Shield-1 for 0–6 h were analysed by immunoblotting with a Ran antibody. Increasing exposure to Shield-1 resulted in increasing levels of DD-Cer-Ran with no change in endogenous Ran protein levels (Fig. 3a). In live cells, upregulation of DD-Cer-Ran protein expression can be observed after only 1 h of incubation with Shield-1 (Fig. 3b–d).

We then tested whether a rapid increase in cytoplasmic DD-Cer-Ran affected ciliary targeting of KIF17. NIH3T3 cells coexpressing KIF17–mCit and DD-Cer-Ran proteins were treated with Shield-1 for 0–4 h and then fixed and stained with antibodies to acetylated and γ-tubulins (Fig. 3e). After 4 h of Shield-1 treatment, increased expression of Ran(T24N) or WT Ran did not affect KIF17–mCit localization (Fig. 3e,f). However, increased expression of GTP-bound Ran(G19V) abolished ciliary localization of KIF17–mCit (Fig. 3e,f). Interestingly, at shorter times of Shield-1 addition and DD-Cer-Ran(G19V) expression, KIF17–mCit localized to more proximal segments of the cilium and/or to the basal body (Fig. 3e, bottom row). Similar results were obtained from live imaging of cells expressing DD-Cer-Ran and monomeric red fluorescent protein (mRFP)–KIF17 constructs (Supplementary Fig. 6). Differences in DD-Cer-Ran(G19V) fluorescence intensity and nuclear localization between fixed (Fig. 3b) and

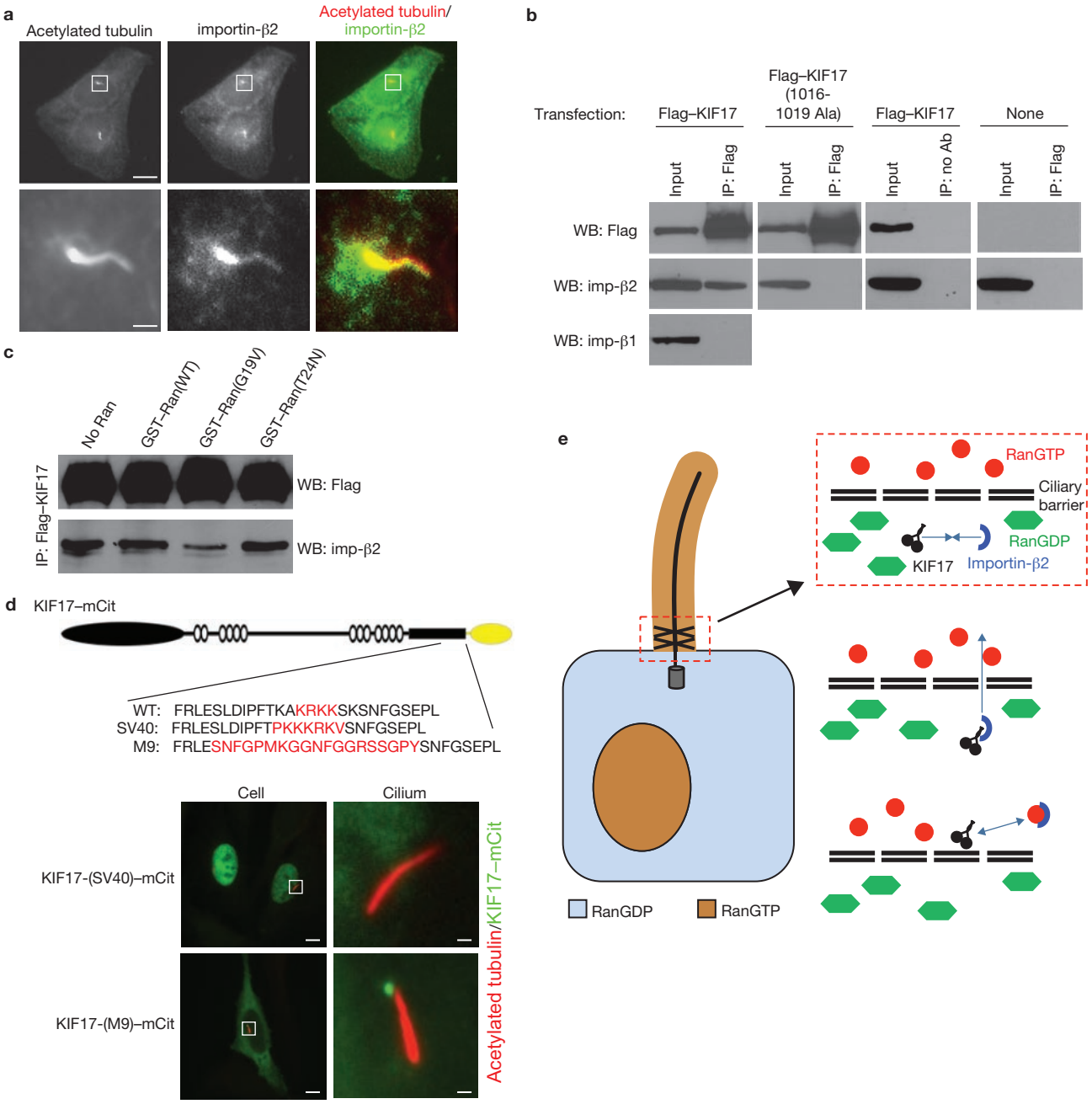

Figure 5 KIF17 forms a complex with importin-β2 that is CLS- and RanGTP-dependent. (**a**) Odora cells were fixed and stained with antibodies to importin-β2 and acetylated tubulin. Top row, images of entire cells; scale bar, 10 μm. Bottom row, magnification of boxed region containing cilia; scale bar, 1 μm. (**b**) Lysates of HEK293T cells expressing Flag-KIF17, Flag-KIF17(1016–1019Ala) or untransfected cells were immunoprecipitated with an anti-Flag antibody. The presence of expressed Flag-KIF17 and endogenous importin-β1 and -β2 proteins in the precipitates was probed by immunoblotting (WB). (**c**) Lysates of HEK293T cells expressing Flag-KIF17 were immunoprecipitated with an anti-Flag antibody in the absence (no Ran) or presence of the indicated purified GST-Ran proteins. The presence of expressed Flag-KIF17 and endogenous importin-β2 proteins in the precipitates was detected by immunoblotting. Uncropped images of western blots are shown in Supplementary Fig. 7. (**d**) Top, schematic of KIF17–mCit constructs in which the CLS is replaced with the NLS from SV40 T-antigen or the M9 NLS from hnRNP A1. Bottom, images of Odora cells expressing KIF17–mCit SV40 or M9 constructs and stained with anti-acetylated-tubulin antibody. Scale bars, 10 μm (left) and 1 μm (right). (**e**) Model for ciliary import of KIF17. In the cytoplasm (top right), KIF17 interacts with importin-β2 in a manner dependent on the KIF17 CLS. The importin/KIF17 complex can shuttle across the ciliary transition zone (middle right) and into the cilium. Once across the barrier (bottom right), the high levels of RanGTP in the cilium cause a dissociation of the KIF17/importin-β2 complex, allowing KIF17 to proceed with its role in IFT. Brown shading in the whole cell depicted on the left indicates subcellular areas of high RanGTP; blue shading, subcellular areas of high RanGDP.

live (Fig. 3e) cells are due to the methanol fixation and immunostaining procedure (Supplementary Fig. 4b). The loss of KIF17–mCit ciliary localization following increased DD-Cer-Ran(G19V) expression is not due to effects of RanGTP on cilia *per se*, as no effect on the presence or length of cilia was observed (Fig. 3g,h). These results show that ciliary KIF17 is dynamic in its location and is mislocalized following an increase in levels

of cytoplasmic RanGTP. We suggest that cytoplasmic RanGTP abolishes ciliary entry of KIF17 and that the dynamic process of IFT allows KIF17 already present in cilia to exit.

To test directly whether Ran controls ciliary entry of KIF17, we performed fluorescence recovery after photobleaching (FRAP) analysis of ciliary KIF17–mCit in the presence or absence of cytoplasmic DD-Cer-Ran(G19V). KIF17–mCit in the distal tips of Odora cilia was photobleached in a single confocal *z*-plane. In the absence of Shield-1, KIF17–mCit fluorescence in the distal tips of cilia recovered to pre-bleach levels within 20 min (Fig. 4a). After 1 h of Shield-1-induced upregulation of DD-Cer-Ran(G19V), little to no recovery of KIF17–mCit fluorescence in the cilium was observed (Fig. 4b). Comparison of fluorescence averages from multiple FRAP experiments revealed a drastic reduction in ciliary KIF17 recovery when Ran(G19V) levels were increased (Fig. 4c). We conclude that the presence of KIF17 in primary cilia is a steady-state process in which motor is entering and leaving the cilium with a constant accumulation at the distal tip, and that entry of KIF17 can be prevented by high levels of cytoplasmic RanGTP.

We next examined whether importin proteins have a role in ciliary entry of KIF17. In nuclear import, NLS-containing proteins form complexes with α- and/or β-importins and are shuttled into the nucleus through NPCs[24,31]. We hypothesized that CLS-containing proteins complex with importins for transport across the ciliary transition zone. This possibility is supported by the presence of α/β-importins in ciliary proteomes from several species[15] and the interaction of the ciliary membrane protein Crumbs3 with importin-β1 during spindle assembly and ciliogenesis[32]. In Odora cells, importin-β2 localized near the nuclear envelope, as expected, as well as near the basal body and in the proximal region of the cilium, consistent with a role for importins in ciliary import (Fig. 5a). KIF17 interacts with importin-β2, as immunoprecipitation of Flag–KIF17 with anti-Flag antibodies resulted in coprecipitation of endogenous importin-β2 (Fig. 5b). The KIF17 CLS is critical for this interaction, as importin-β2 was not coprecipitated with the 1016–1019ala mutant (Fig. 5b). The observations that mutation of the KIF17 CLS (amino acids 1016–1019) interfered with both ciliary entry (Fig. 1) and importin-β2 binding (Fig. 5b) indicate that interaction with importin-β2 is necessary for ciliary entry of KIF17. After crossing the ciliary transition zone, RanGTP in the cilium could cause dissociation of KIF17 from importin-β2, freeing the motor for IFT. Indeed, addition of recombinant glutathione *S*-transferase (GST)–Ran(G19V) to cell lysates before immunoprecipitation reduced the KIF17/importin-β2 interaction, whereas addition of WT Ran or Ran(T24N) had no effect (Fig. 5c).

As the primary sequence of the KIF17 CLS is similar to classical NLSs that interact with importin-β1, the interaction of KIF17 with importin-β2 was surprising. However, no interaction between KIF17 and importin-β1 was observed by immunoprecipitation (Fig. 5b). Also, similarities can be found between the KIF17 CLS and the basic-enriched/PY subclass of consensus sequences for importin-β2 binding[23]. To directly compare roles of importins β1 and β2 in ciliary entry of KIF17, we replaced the KIF17 CLS with NLSs known to interact with either importin-β1 or importin-β2. KIF17–mCit still localized to primary cilia when its CLS was replaced with the M9 NLS from hnRNP A1, which interacts with importin-β2 (Fig. 5d). In contrast, KIF17–mCit was targeted to the nucleus when its CLS was replaced with the NLS from the SV-40 large T-antigen, which interacts with importins α and β1 (Fig. 5d). These results suggest that importin-β2 alone is responsible for ciliary entry of KIF17.

In conclusion, we propose a model for ciliary import (Fig. 5e) in which cytoplasmic KIF17 interacts with importin-β2 (Fig. 5e, top right). This complex crosses the ciliary transition zone (Fig. 5e, middle right) and is dissociated by RanGTP in the proximal cilium (Fig. 5e, bottom right), allowing KIF17 to proceed with its role in IFT. Perturbation of the RanGTP/GDP gradient prevented ciliary entry of KIF17, presumably by inhibiting formation of KIF17/importin complexes before transport across the ciliary transition zone. These results provide the first direct evidence that ciliary and nuclear import pathways use similar mechanisms. In addition, Ran and importin proteins regulate the localization and activation of kinesin motors during spindle assembly in mitotic cells[33,34], and our work expands the role of Ran to include global regulation of kinesin compartmentalization in interphase cells.

How proteins gain access to the ciliary compartment has been unclear. Sequences critical for ciliary targeting of membrane proteins (for example, VxPx, RVxP and Ax(S/A)xQ) are known[13,35,36] but it is unclear how these sequences function, as several pathways have been described for trafficking of membrane proteins to the cilium[9,37–39]. Here we describe a new entry pathway for cytoplasmic kinesin motors analogous to nuclear entry of proteins. Whether importin- and Ran-regulated import pathways regulate entry of other motors and their cargoes at the ciliary transition zone requires further analysis.

It is interesting to note that the KIF17 CLS can function as a CLS or an NLS depending on protein context. Several NLS-like sequences have been found on the KIF3A/KIF3B/KAP complex, and the KAP subunit has been observed to redistribute from cilia to nuclei during the mitotic cycle[40]. It is likely that additional signals in KIF17 are required to promote ciliary rather than nuclear import. One possibility is that KIF17 motor activity along cytoplasmic and/or centriole microtubules is needed to position the CLS-containing protein at the ciliary base rather than the nuclear envelope. Alternatively, cargo and/or membrane binding may be required for ciliary entry. Further experiments are required to test these possibilities as well as the global role of importins and Ran in ciliary entry. □

ACKNOWLEDGEMENTS

This work was supported by NIH grants R01GM070862 and R01GM083254 (to K.J.V.), R01DC009606 (to J.R.M.), R01DK084725 (to B.M.), and T32GM007767 and T32DC00011 (to P.M.J.). Work was also supported by NRSAs F32GM089034 (to J.F.D.) and F31DC009524 (to P.M.J.). H.L.K. is supported as a Barbour Fellow at the University of Michigan. pGEX-Ran plasmids were a kind gift from Brian Burke (University of Florida) and rabbit anti-RanGTP antibody was a kind gift from Ian Macara (University of Virginia).

AUTHOR CONTRIBUTIONS

J.F.D., H.L.K, P.M.J., S.F. and Y.N.T. performed experiments. J.F.D., H.L.K., P.M.J., J.R.M. and K.J.V. designed experiments. All authors contributed to helpful discussions shaping the aims of the project. J.F.D and K.J.V. wrote the manuscript, with all authors providing detailed comments and suggestions. K.J.V. directed the project.

COMPETING FINANCIAL INTERESTS

The authors declare no competing financial interests.

Published online at http://www.nature.com/naturecellbiology
Reprints and permissions information is available online at http://npg.nature.com/reprintsandpermissions/

1. Silverman, M. A. & Leroux, M. R. Intraflagellar transport and the generation of dynamic, structurally and functionally diverse cilia. *Trends Cell Biol.* **19**, 306–316 (2009).
2. Scholey, J. M. Intraflagellar transport motors in cilia: moving along the cell's antenna. *J. Cell Biol.* **180**, 23–29 (2008).
3. Satir, P., Mitchell, D. R. & Jekely, G. How did the cilium evolve? *Curr. Top. Dev. Biol.* **85**, 63–82 (2008).
4. Gerdes, J. M., Davis, E. E. & Katsanis, N. The vertebrate primary cilium in development, homeostasis, and disease. *Cell* **137**, 32–45 (2009).

5. Satir, P. & Christensen, S. T. Overview of structure and function of mammalian cilia. *Annu. Rev. Physiol.* **69**, 377–400 (2007).
6. Scholey, J. M. & Anderson, K. V. Intraflagellar transport and cilium-based signaling. *Cell* **125**, 439–442 (2006).
7. Tobin, J. L. & Beales, P. L. The nonmotile ciliopathies. *Genet. Med.* **11**, 386–402 (2009).
8. Fliegauf, M., Benzing, T. & Omran, H. Mechanisms of disease - when cilia go bad: cilia defects and ciliopathies. *Nat. Rev. Mol. Cell Biol.* **8**, 880–893 (2007).
9. Rosenbaum, J. L. & Witman, G. B. Intraflagellar transport. *Nat. Rev. Mol. Cell Biol.* **3**, 813–825 (2002).
10. Ou, G. S., Blacque, O. E., Snow, J. J., Leroux, M. R. & Scholey, J. M. Functional coordination of intraflagellar transport motors. *Nature* **436**, 583–587 (2005).
11. Snow, J. J. *et al.* Two anterograde intraflagellar transport motors cooperate to build sensory cilia on *C. elegans* neurons. *Nat. Cell Biol.* **6**, 1109–1123 (2004).
12. Insinna, C., Pathak, N., Perkins, B., Drummond, I. & Besharse, J. C. The homodimeric kinesin, Kif17, is essential for vertebrate photoreceptor sensory outer segment development. *Dev. Biol.* **316**, 160–170 (2008).
13. Jenkins, P. M. *et al.* Ciliary targeting of olfactory CNG channels requires the CNGB1b subunit and the kinesin-2 motor protein, KIF17. *Curr. Biol.* **16**, 1211–1216 (2006).
14. Insinna, C., Humby, M., Sedmak, T., Wolfrum, U. & Besharse, J. C. Different roles for KIF17 and kinesin II in photoreceptor development and maintenance. *Dev. Dynam.* **238**, 2211–2222 (2009).
15. Gherman, A., Davis, E. E. & Katsanis, N. The ciliary proteome database: an integrated community resource for the genetic and functional dissection of cilia. *Nat. Genet.* **38**, 961–962 (2006).
16. Gilula, N. B. & Satir, P. The ciliary necklace. A ciliary membrane specialization. *J. Cell Biol.* **53**, 494–509 (1972).
17. Luby-Phelps, K., Fogerty, J., Baker, S. A., Pazour, G. J. & Besharse, J. C. Spatial distribution of intraflagellar transport proteins in vertebrate photoreceptors. *Vision Res.* **48**, 413–423 (2008).
18. Deane, J. A., Cole, D. G., Seeley, E. S., Diener, D. R. & Rosenbaum, J. L. Localization of intraflagellar transport protein IFT52 identifies basal body transitional fibers as the docking site for IFT particles. *Curr. Biol.* **11**, 1586–1590 (2001).
19. Murrell, J. R. & Hunter, D. D. An olfactory sensory neuron line, Odora, properly targets olfactory proteins and responds to odorants. *J. Neurosci.* **19**, 8260–8270 (1999).
20. Jekely, G. & Arendt, D. Evolution of intraflagellar transport from coated vesicles and autogenous origin of the eukaryotic cilium. *Bioessays* **28**, 191–198 (2006).
21. Devos, D. *et al.* Components of coated vesicles and nuclear pore complexes share a common molecular architecture. *PLOS biol.* **2**, 2085–2093 (2004).
22. Christensen, S. T., Pedersen, L. B., Schneider, L. & Satir, P. Sensory cilia and integration of signal transduction in human health and disease. *Traffic* **8**, 97–109 (2007).
23. Lee, B. J. *et al.* Rules for nuclear localization sequence recognition by karyopherin beta 2. *Cell* **126**, 543–558 (2006).
24. Stewart, M. Molecular mechanism of the nuclear protein import cycle. *Nat. Rev. Mol. Cell Biol.* **8**, 195–208 (2007).
25. Liu, Q. *et al.* The proteome of the mouse photoreceptor sensory cilium complex. *Mol. Cell. Proteomics* **6**, 1299–1317 (2007).
26. Richards, S. A., Lounsbury, K. M. & Macara, I. G. The C terminus of the nuclear RAN/TC4 GTPase stabilizes the GDP-bound state and mediates interactions with RCC1, Ran-GAP, and HTF9A/RanBP1. *J. Biol. Chem.* **270**, 14405–14411 (1995).
27. Lounsbury, K. M., Richards, S. A., Carey, K. L. & Macara, I. G. Mutations within the Ran/TC4 GTPase - Effects on regulatory factor interactions and subcellular localization. *J. Biol. Chem.* **271**, 32834–32841 (1996).
28. Banaszynski, L. A., Chen, L. C., Maynard-Smith, L. A., Ooi, A. G.L. & Wandless, T. J. A rapid, reversible, and tunable method to regulate protein function in living cells using synthetic small molecules. *Cell* **126**, 995–1004 (2006).
29. Maynard-Smith, L. A., Chen, L. C., Banaszynski, L. A., Ooi, A. G.L. & Wandless, T. J. A directed approach for engineering conditional protein stability using biologically silent small molecules. *J. Biol. Chem.* **282**, 24866–24872 (2007).
30. Schoeber, J. P. H. *et al.* Conditional fast expression and function of multimeric TRPV5 channels using Shield-1. *Am. J. Physiol. Renal Physiol.* **296**, F204–F211 (2009).
31. Weis, K. Regulating access to the genome: nucleocytoplasmic transport throughout the cell cycle. *Cell* **112**, 441–451 (2003).
32. Fan, S. L. *et al.* A novel Crumbs3 isoform regulates cell division and ciliogenesis via importin beta interactions. *J. Cell Biol.* **178**, 387–398 (2007).
33. Ems-McClung, S. C., Zheng, Y. X. & Walczak, C. E. Importin alpha/beta and Ran-GTP regulate XCTK2 microtubule binding through a bipartite nuclear localization signal. *Mol. Biol. Cell* **15**, 46–57 (2004).
34. Tahara, K. *et al.* Importin-beta and the small guanosine triphosphatase Ran mediate chromosome loading of the human chromokinesin Kid. *J. Cell. Biol.* **180**, 493–506 (2008).
35. Mazelova, J. *et al.* Ciliary targeting motif VxPx directs assembly of a trafficking module through Arf4. *EMBO J.* **28**, 183–192 (2009).
36. Geng, L. *et al.* Polycystin-2 traffics to cilia independently of polycystin-1 by using an N-terminal RVxP motif. *J. Cell. Sci.* **119**, 1383–1395 (2006).
37. Pazour, G. J. & Bloodgood, R. A. Targeting proteins to the ciliary membrane. *Curr. Top. Dev. Biol.* **85**, 115–149 (2008).
38. Hunnicutt, G. R., Kosfiszer, M. G. & Snell, W. J. Cell body and flagellar agglutinins in *Chlamydomonas reinhardtii* - the cell body plasma-membrane is a reservoir for agglutinins whose migration to the flagella is regulated by a functional barrier. *J. Cell. Biol.* **111**, 1605–1616 (1990).
39. Casanova, J. E. *et al.* Association of Rab25 and Rab11a with the apical recycling system of polarized Madin-Darby canine kidney cells. *Mol. Biol. Cell* **10**, 47–61 (1999).
40. Morris, R. L. *et al.* Redistribution of the kinesin-II subunit KAP from cilia to nuclei during the mitotic and ciliogenic cycles in sea urchin embryos. *Dev. Biol.* **274**, 56–69 (2004).

METHODS

Antibodies and plasmids. Commercial antibodies include: γ-tubulin (polyclonal and GTU-88 clone, Sigma), Myc (9E10 clone, Sigma), importin-β2 (558660, BD Pharmingen), importin-β1 (610559, BD Transduction Laboratories), Flag (F7425 or M2 clone, Sigma), Ran (610340, BD Transduction Laboratories) and adenylyl cyclase III (Santa Cruz Biotechnology). The rabbit polyclonal antibody to acetylated tubulin was raised against an acetylated α-tubulin peptide CGQMPSD(AcK)TIGGGDD. The rabbit anti-RanGTP antibody was a kind gift from Ian Macara (University of Virginia). Secondary antibodies for immunoblotting and immunofluorescence were from Jackson ImmunoResearch and Invitrogen.

Tagged versions of full-length human KIF17 (NP_065867) were created in pmCit-N1 and pmCit–C1 (ref. 41), pCDNA3-Flag or pRK5-Myc using convenient restriction sites or PCR. Truncated versions were created by PCR using primers with appropriate restriction sites for subcloning back into the appropriate vector. All mutagenesis was performed using the Quickchange kit (Stratagene). Wild-type and mutant KIF17 tail domains were amplified by PCR and inserted in frame between the KHC (rat KIF5C) and mCit coding sequences in the plasmid KHC-mCitN1 (ref. 41). Plasmids for bacterial expression of wild-type and mutant Ran proteins were a gift from Brian Burke (University of Florida). The Ran coding sequences were subcloned into plasmids pCer-C1 and pRK5–Myc to create Cerulean and Myc-tagged versions, respectively, for expression in mammalian cells. The destabilization domain (FKBP-L106P, Clontech Proteotuner System) was then inserted upstream of Cer to create the DD-Cer-Ran constructs.

Cell culture and transfection. MDCK II cells are dog kidney epithelial cells commonly used to study the formation and functioning of primary cilia. hTERT-RPE cells are from mouse retinal pigment epithelium immortalized with human telomerase. NIH3T3 are derived from NIH Swiss mouse embryo cultures. Odora cells are SV40-immortalized cells from rat olfactory epithelium.

Odora, NIH3T3, HEK293T, and COS cells were grown in DMEM (Gibco) supplemented with 10% fetal clone III (Hyclone) and 1% GlutaMAX (Gibco). Cells were transfected using either Trans-IT (Mirus) or ExpressFect (Denville) transfection reagents and typically used for experiments 24 h after transfection. NIH3T3 cells were serum starved for 24–48 h to induce ciliogenesis before transfection. MDCK II cells were grown in DMEM buffer supplemented with 10% foetal bovine serum and 1% GlutaMAX and transfected using Lipofectamine (Invitrogen) in Opti-MEM (Gibco). hTERT-RPE cells were grown in DMEM/F12 media (Gibco) supplemented with 10% FBS and 0.01 mg/ml hygromycin B, transfected with Trans-IT transfection reagent and serum starved for 24–48 h to induce ciliogenesis.

Isolation of cilia from rat olfactory epithelium. Female Sprague-Dawley rats were obtained from Harlan and were used in the isolation of primary cilia from the rat olfactory epithelium. All experimental procedures were approved by the University of Michigan Committee on the Use and Care of Animals and performed in accordance with the Guide for the Care and Use of Laboratory Animals, as adopted and promulgated by the National Institutes of Health.

Olfactory cilia were isolated using a combination of the calcium-shock method[42] followed by NaBr treatment[43], with minor modifications. The olfactory epithelia from seven rats were surgically removed, washed in ice-cold Ringer's Solution (120 mM NaCl, 5 mM KCl, 1.6 mM K_2HPO_4, 25 mM $NaHCO_3$, 7.5 mM D-glucose and 5 mM EGTA) and then placed in deciliation solution (Ringer's Solution containing complete protease inhibitor cocktail (Roche Applied Science), 20 mM $CaCl_2$ and 30 mM KCl)). Cilia were detached by gentle agitation for 20 min at 4 °C and isolated by multiple centrifugation steps in a 45% w/v sucrose solution. Cilia visible as a white layer at the sucrose-supernatant interface were extracted and diluted in ten-fold volume of deciliation solution and then pelleted. The cilia pellet was resuspended in a NaBr solution and centrifuged again. This was repeated once more before the final cilia pellet was resuspended in washing solution (10 mM Tris, 3 mM $MgCl_2$ and 2 mM EGTA), centrifuged a final time and then analysed by SDS–polyacrylamide gel electrophoresis (SDS–PAGE) and western blot.

Deciliated lysates were prepared from tissue remaining after deciliation. The tissue was homogenized using a dounce homogenizer in deciliation solution. Insoluble material was removed by centrifugation and supernatant portions were analysed by SDS–PAGE and western blot.

Deciliation was verified by scanning electron microscopy. Olfactory epithelia were removed from euthanized animals, washed in ice-cold Ringer's Solution and either immediately placed in fixative solution (8% glutaraldehyde, 0.6 M cacodylate) for 24 h at 4 °C or deciliated by gentle agitation in deciliation solution and then subsequently placed in fixative solution for 24 h at 4 °C. Epithelia were then processed using the OTOTO method[44]. Samples were dehydrated in a graded series of increasing ethanol concentrations, critical point dried and mounted on stubs using silver paste. Samples were analysed using an AMRAY 1910 field emission scanning electron microscope.

Immunofluorescence and immunohistochemistry. For immunofluorescence, cells were fixed in either methanol at –20 °C or 3.7% paraformaldehyde followed by 50 mM NH_4Cl at room temperature. Samples were permeabilized with 0.2% TX-100 for 5 min and then briefly blocked with 0.2% fish skin gelatin (Sigma) in PBS buffer before addition of primary and secondary antibodies. For immunostaining with the anti-RanGTP antibody, cells were permeabilized with 0.05% TX-100 to enable good visualization of ciliary-localized proteins. Permeabilization with higher levels of TX-100 (0.1% or 0.25%) allowed nuclear staining (Supplementary Fig. 5b) but somewhat inhibited visualization of RanGTP in the ciliary compartment.

For immunohistochemistry, olfactory epithelia were removed from animals euthanized by cardiac perfusion with PBS followed by 4% paraformaldehyde, post-fixed in 4% paraformaldehyde for 4 h and incubated in 30% sucrose solution for 24 h at 4 °C. After incubation, samples were frozen in OCT compound (Sakura Finetek) and cut into sections (20 μm on a cryostat. Epithelium tissue was incubated with 1% SDS for 10 min and washed with PBS before incubation with primary and secondary antibodies.

All samples were mounted with ProLong Gold (Invitrogen). Images were obtained on an inverted epifluorescence microscope (TE2000-E, Nikon) or a confocal imaging system (FluoView 500, Olympus) and analysed with ImageJ (NIH) or MetaMorph software (Molecular Devices). Tissue images were obtained by taking a series of images, one every 0.5 μm through the epithelium, and combining the images into a composite stack (a *z*-series).

Immunoprecipitation. HEK293T cell lysate was prepared in lysis buffer (25 mM HEPES, 115 mM potassium acetate, 5 mM sodium acetate, 5 mM $MgCl_2$, 0.5 mM EGTA and 1% TX-100) and protease inhibitors (1 mM). Lysates were cleared twice before addition of antibody alone or 5 μg recombinant Ran proteins at 4 °C. Immunoprecipitates were recovered with protein A agarose beads (Invitrogen), washed at least twice in lysis buffer and analysed by SDS–PAGE and western blotting.

Purification of bacterially expressed proteins. Expression of GST-tagged Ran(WT), Ran(G19V) and Ran(T24N) proteins in BL21 (DE3) cells was induced with 100 μM isopropylthiogalactoside (IPTG) for 2 h at 37 °C. After lysis, the GST-tagged proteins were purified using glutathione Sepharose beads (GE Healthcare). Purified proteins were dialysed overnight in 10 mM Tris at pH 7.4, 150 mM NaCl, 1 mM EDTA, 1 mM dithiothreitol and 5% glycerol. Protein concentration was determined by Bradford assay.

DD-Ran experiments. For fixed cell experiments, serum starved NIH3T3 cells were transfected with DD-Cer-Ran and KIF17 constructs for 24 h before addition of Shield-1 for 0–4 h, then fixed, permeabilized and immunostained. Cilium lengths were determined with MetaMorph software by tracing the midline of primary cilia visualized with acetylated tubulin antibody.

For live cell DD-Ran experiments, cells were plated in glass-bottomed dishes (MatTek), serum starved for 24–48 h and transfected. Immediately before imaging, cells were put into a pre-warmed HEPES buffer (25 mM HEPES, 115 mM potassium acetate, 5 mM sodium acetate, 5 mM $MgCl_2$ and 2 mM EGTA) supplemented with Shield-1. Cells chosen for experiments were morphologically normal and presented good expression of KIF17 along the length of primary cilia. An objective heater (Bioptechs) was used to warm cells. Images were taken every 10 min for up to 4 h and analysed with ImageJ.

For FRAP experiments, Odora cells in glass-bottomed dishes expressing KIF17–mCit and DD-Cer-Ran(G19V) were imaged on an Olympus FluoView confocal system using a live cell imaging chamber to maintain appropriate temperature and atmosphere. Cells were imaged either before or 1 h after the addition of Shield-1 directly to cell medium. Distal tips of cilia were photobleached using 100% laser power for 90 s, and recovery images were taken at 1 min intervals for 20 min at 10% laser power. Fluorescence data was subjected to background sub-

DOI: 10.1038/ncb2073

traction and normalized for additional photobleaching during recovery. Averaged data was plotted and fitted to single exponential functions in Prism software (Graphpad Software).

Statistical analysis. All statistical analysis was performed using Prism software and specific tests are noted in the text. Unless otherwise noted, all error bars represent ± s.e.m. and significance was assessed as $p < 0.05$.

41. Cai, D. W., Hoppe, A. D., Swanson, J. A. & Verhey, K. J. Kinesin-1 structural organization and conformational changes revealed by FRET stoichiometry in live cells. *J. Cell. Biol.* **176**, 51–63 (2007).
42. Mayer, U. *et al.* Proteomic analysis of a membrane preparation from rat olfactory sensory cilia. *Chem. Senses* **33**, 145–162 (2008).
43. Mayer, U. *et al.* The proteome of rat olfactory sensory cilia. *Proteomics* **9**, 322–334 (2009).
44. Davies, S. & Forge, A. Preparation of the mammalian organ of Corti for scanning electron-microscopy. *J. Microsc-Oxford* **147**, 89–101 (1987).

nature cell biology

DOI: 10.1038/ncb2073

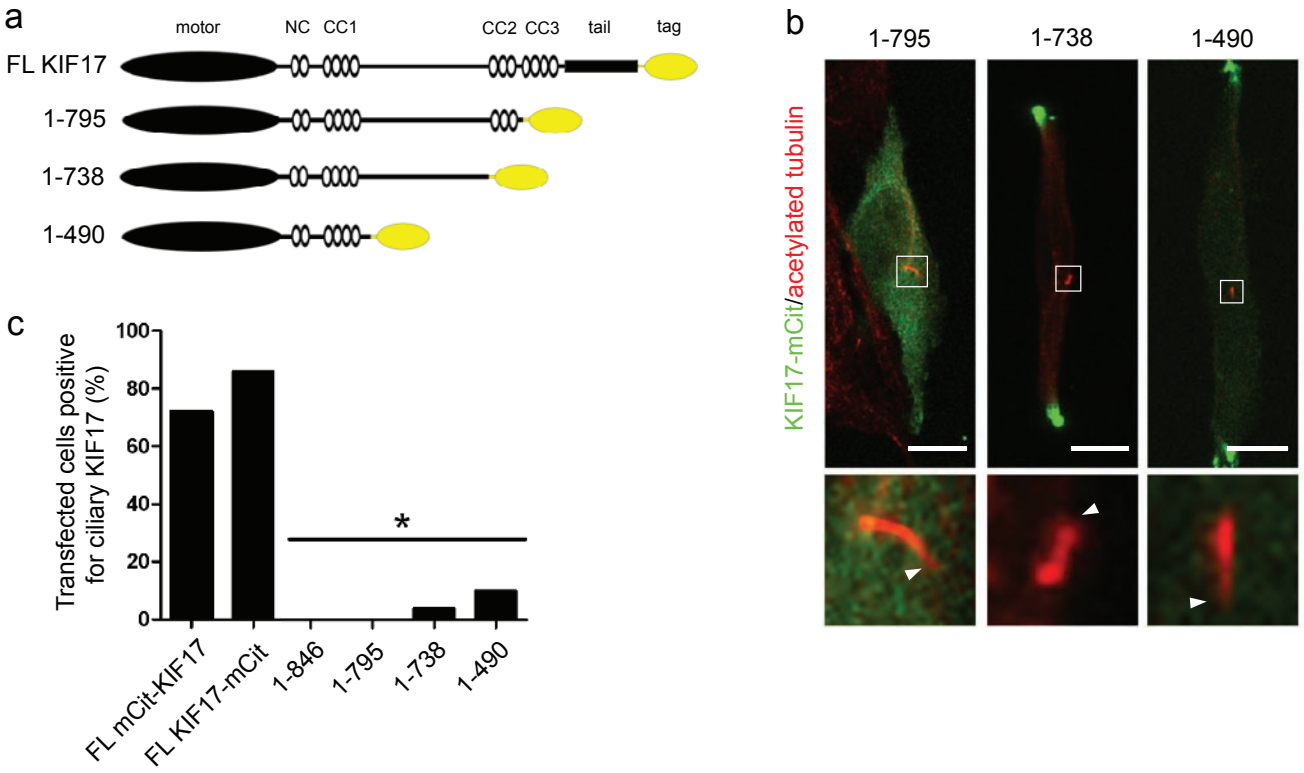

Figure S1 C-terminal truncations abolish ciliary targeting of KIF17. (**a**) Schematic of full length and truncated forms of human KIF17. NC, neck coil; CC, coiled coil. (**b**) Immunofluorescence images of fixed Odora cells expressing the indicated KIF17-mCit truncations (green) and stained with an antibody to acetylated tubulin (red) to mark primary cilia. Top row, images of entire cells (scale bar, 10 μm); bottom row, magnifcation of boxed regions containing cilia. White arrowhead indicates distal tips of cilia. (**c**) Quantification of the results in Fig. 1b, 1c and S1b to determine the ciliary localization of full length and truncated versions of KIF17. $n = 50$ for each KIF17 construct. Deletion of the KIF17 tail domain abolishes ciliary localization (Fig. 1c). Further truncations that remove sections of the stalk domain also fail to localize to cilia even though the (1-795) and (1-490) constructs are active for motility along cytoplasmic microtubules (**b**). That both mCit-KIF17 and KIF17-mCit localize to the distal tips of cilia demonstrates that placement of the mCit tag (i.e. N- or C-terminus) has no effect on ciliary targeting. *, $p<0.0001$ vs. full length KIF17 (Fisher's Exact test).

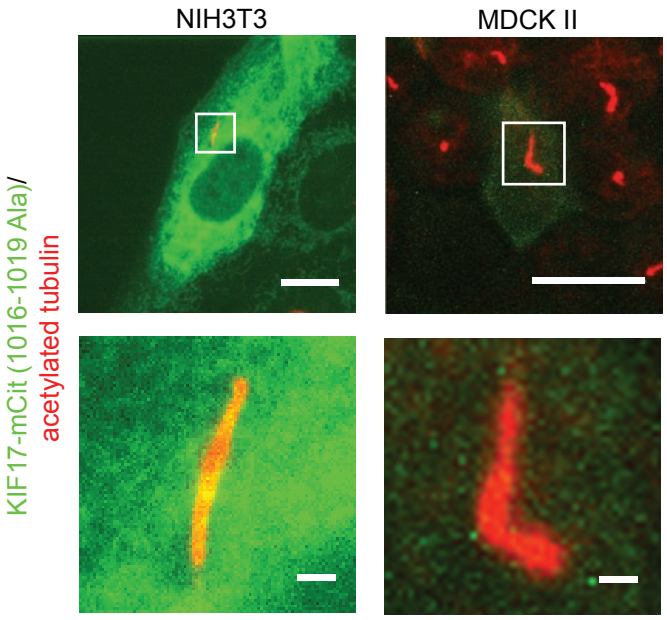

Figure S2 The KIF17 CLS is necessary for ciliary localization. Immunofluorescence images of fixed NIH3T3 and MDCK II cells expressing KIF17-mCit(1016-1019 ala) (green) and stained with an antibody to acetylated tubulin (red). Top row, images of whole cells (scale bars, 10 μm); bottom row, magnification of boxed areas containing cilia (scale bars, 1 μm). Mutation of the CLS (aa1016-1019) abolishes localization of KIF17 to primary cilia.

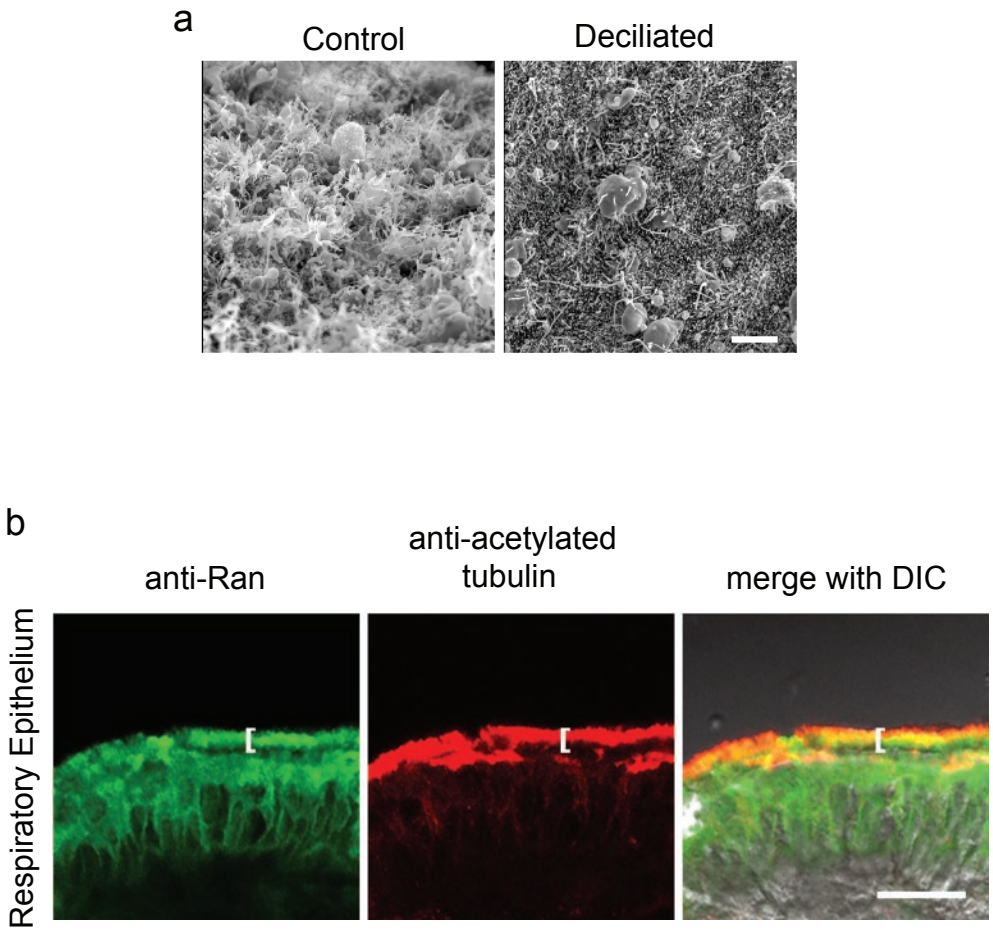

Figure S3 Localization of Ran in the ciliary compartment. (**a**) SEM images demonstrate the removal of cilia from the apical surface of rat olfactory epithelium. Untreated olfactory epithelium (Control) or epithelium treated with deciliation solution (Decilated) were fixed and stained for SEM at 2,700x magnification. Scale bar,10 µm. (**b**) Representative compressed confocal stacks of coronal sections of rat respiratory epithelium. Respiratory epithelia were immunostained with antibodies directed against Ran (left, green) and acetylated tubulin (middle, red). Merged imaged with Differential Interference Contrast (DIC) image is shown on right. Scale bars, 20 µm. Brackets denote cilia layer.

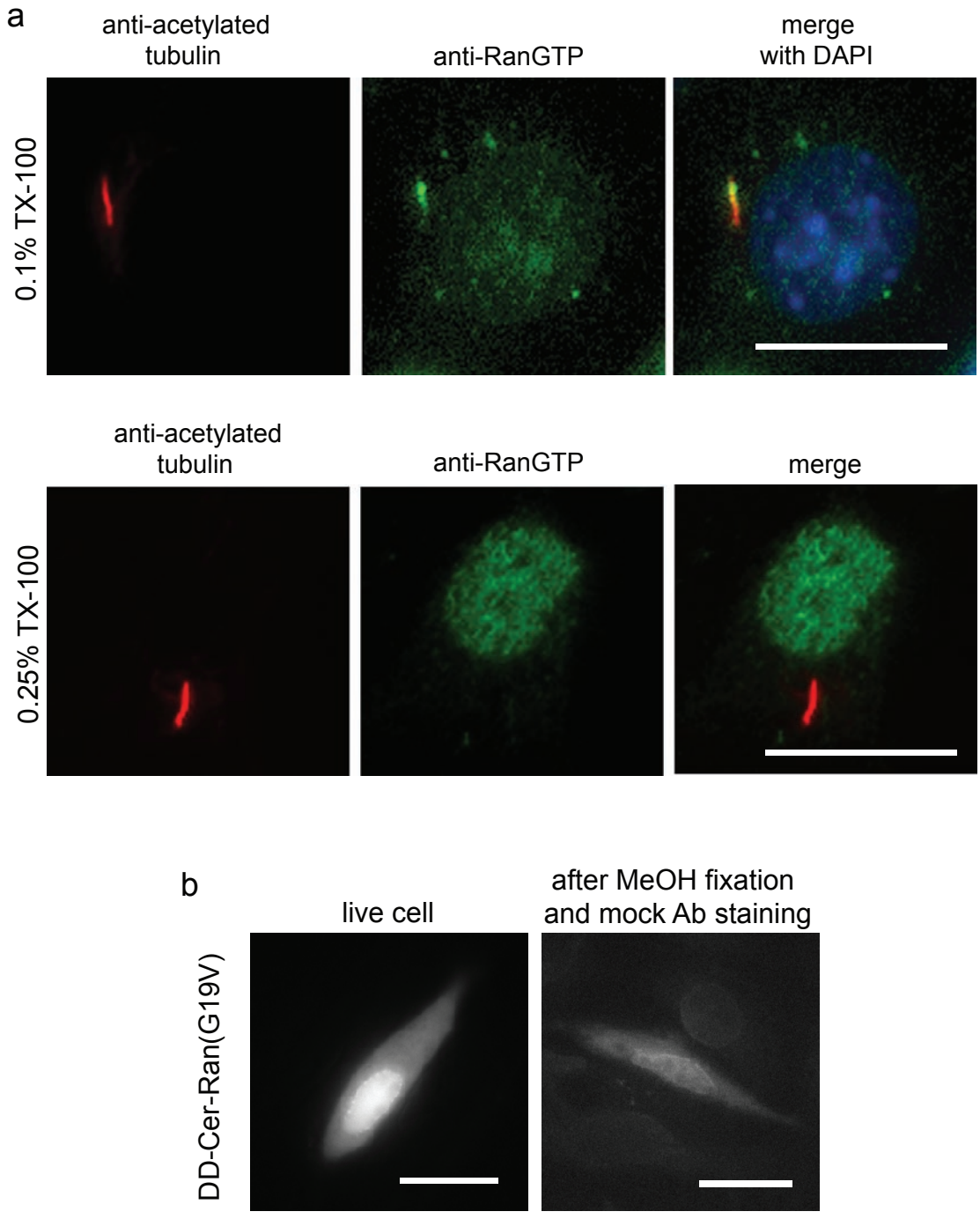

Figure S4 Variations in fixation and immunostaining procedures can affect visualization of nuclear and ciliary Ran. (**a**) Fluorescence images of NIH3T3 cells stained with anti-RanGTP antibody. Permeabilization with 0.1% TX-100 resulted in staining of RanGTP in both ciliary and nuclear compartments whereas permeabilization with 0.25% TX-100 yielded fluorescence signal only from the nucleus. Scale bars, 10 μm. (**b**) Fluorescence images of live and methanol-fixed cells expressing DD-Cer-Ran(G19V). NIH3T3 cells expressing DD-Cer-Ran(G19V) were treated with Shield-1 for 1 h and then imaged live (left) or fixed with methanol and subjected to a mock immunofluorescence protocol (permeabilization, two antibody incubation steps, and multiple wash steps) (right). DD-Cer-Ran(G19V) showed higher fluorescence and greater nuclear localization in live cells than in fixed cells. Scale bar, 10 μm.

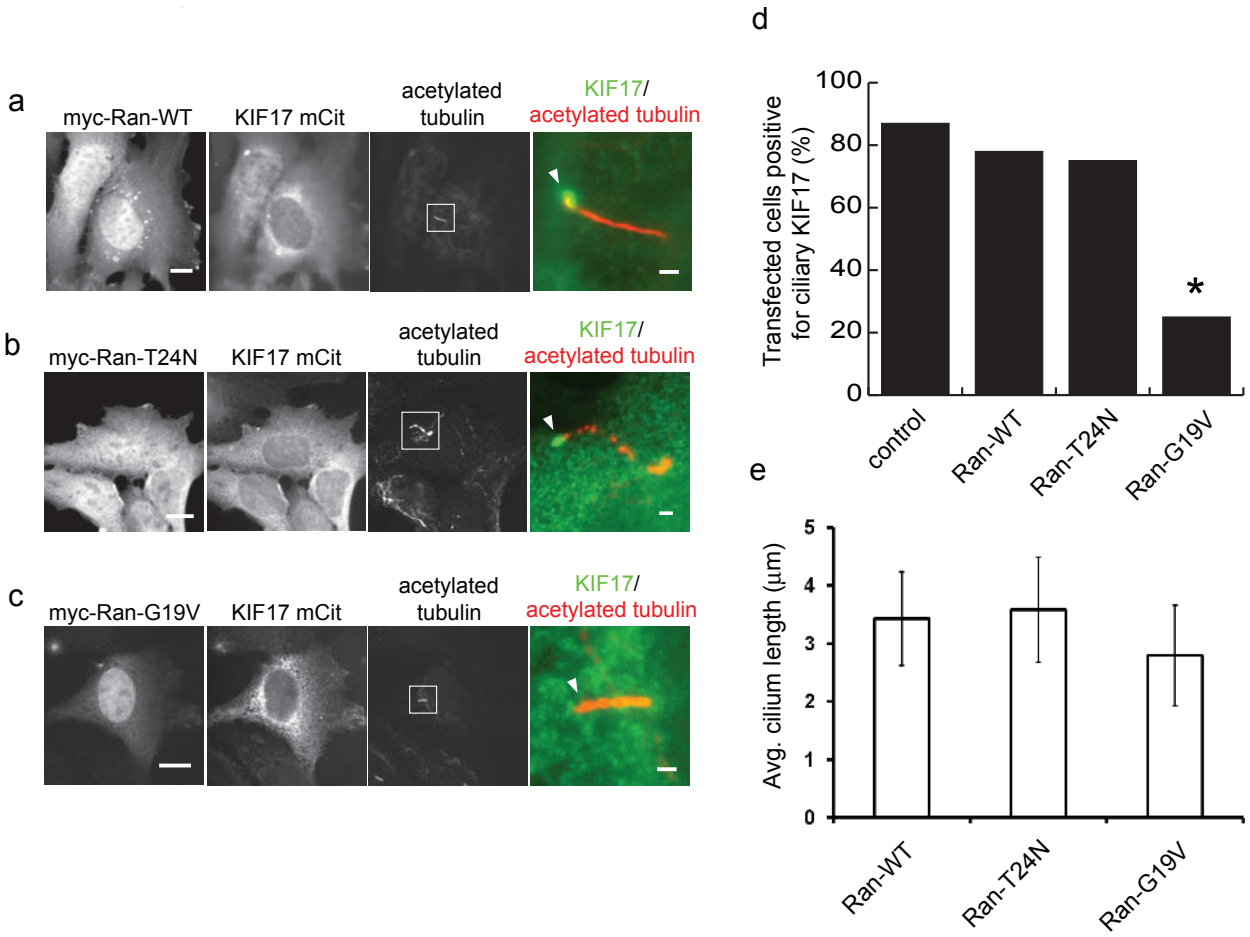

Figure S5 Overexpression of constitutively active Ran inhibits ciliary localization of KIF17. (**a-c**) Immunofluorescence images of serum starved NIH3T3 cells co-expressing KIF17-mCit and myc-Ran (WT or mutants) overnight and then fixed and stained for acetylated tubulin to mark the primary cilia. White arrowheads indicate distal tips of cilia. Expression of Ran(G19V) (**c**), but not WT (**a**) or T24N (**b**), resulted in significantly fewer cells with ciliary localization of KIF17-mCit as determined by quantification (**d**). * $p<0.0001$ vs. control (Fisher's Exact test). $n = 30$ for each condition. (**e**) Quantification of average cilia length in cells expressing the myc-Ran constructs. Error bars are ±SD.

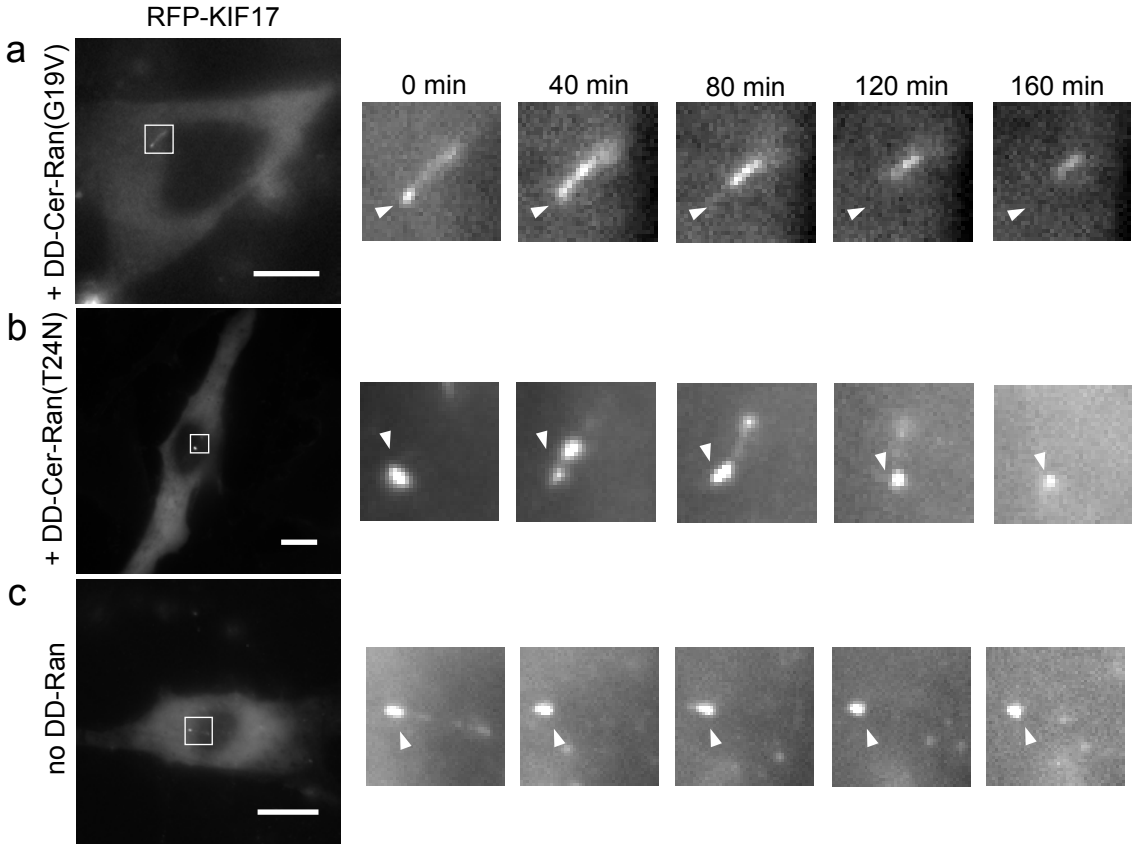

Figure S6 Live-cell imaging of KIF17 localization in cilia upon DD-Cer-Ran(G19V) upregulation. (**a-c**) NIH3T3 cells expressing (c) KIF17-mCit alone or together with (a) DD-Cer-Ran(G19V) or (b) DD-Cer-Ran(T24N) were imaged live before (left panels) or at the indicated times after Shield-1 addition (right panels showing magnification of white boxed regions containing cilia). Increased expression of DD-Cer-Ran(G19V) resulted in a decrease in KIF17-mCit fluorescence in cilia tips (a) whereas expression of DD-Cer-Ran(T24N) (**b**) or no DD-Cer-Ran protein (**c**) cells resulted in no change in KIF17-mCit localization to the distal tips of cilia. Arrowheads indicate distal tips of cilia.

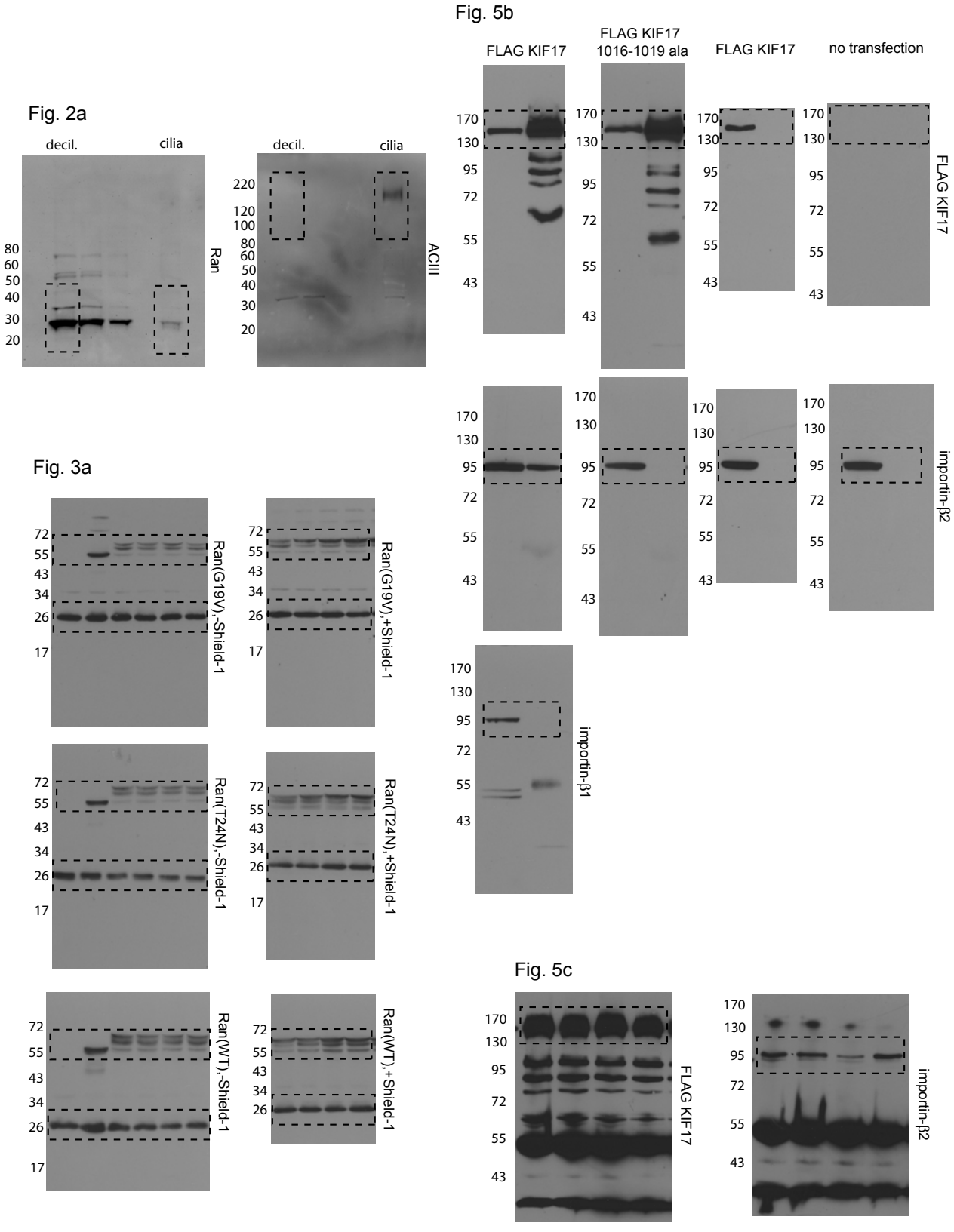

Figure S7 Uncropped images of western blots. Boxed areas indicate regions depticted in main text figures. The additional bands seen in Flag-KIF17 immunoprecipitation blots (Figure 5b,c) are likely degraded KIF17. The ~55kDa and 40kDa background bands in Figure 5c are the IgG heavy and light chains from the anti-Flag antibody used for immunoprecipitation.